Reprinted from Applied Optics, Vol. 24, page 2362, August 1, 1985

High-speed high-resolution fiber diameter variation measurement system

Martin M. Fejer, Gregory A. Magel, and Robert L. Byer

A fiber diameter variation measurement system is described which is capable of measuring transparent fibers with 0.02% diameter resolution and 6-μm axial resolution at a measurement rate of 1 kHz and with a working distance of >100 mm. The principles of its operation are discussed in detail, and experimental confirmation of its performance is reported. A theoretical calculation of the optimum obtainable diameter resolution for a given set of experimental parameters is also presented.

I. Introduction

There is considerable current interest in the growth and application of single crystal fibers for nonlinear optical, miniature laser, and acoustic devices.[1-4] Our efforts to apply the miniature pedestal growth technique[1,5] to the growth of refractory oxide fibers have shown that closed-loop control of the fiber diameter is necessary to achieve the diameter control requisite for useful device applications.

The crystal growth process involves melting the tip of a source rod with a tightly focused CO_2 laser, dipping the seed crystal into the melt, and then effecting a diameter reduction by pulling the seed more rapidly than feeding in the source. Since there is no viscous drawdown region, small scale diameter variations tend to be frozen into the fiber instead of being stretched to long periods and low amplitudes as in glass fiber pulling. It is thus necessary to measure the fiber diameter with high axial resolution in addition to good diameter resolution. The CO_2 laser focusing optics and the short thermal time constant of the molten zone impose additional constraints on the working distance and measurement rate.

While the diameter control tolerances and the growth parameters depend in detail on the material and device application involved, the following criteria specify a measurement system useful for a broad range of crystal fiber applications: diameter variation resolution better than 0.1% for fiber diameters between 20 and 500 μm; axial resolution better than 10 μm; working distance >100 mm; and measurement rate faster than 100 Hz.

The forward scattering pattern from a fiber illuminated by a laser beam perpendicular to the fiber axis can be used to measure the diameter of the fiber.[6] A fiber diameter measurement device based on counting the number of fringes scattered into a particular angular range has been described previously.[7] While the speed and resolution of the above system are suitable for our application, the optical system for imaging the requisite large 60° angular range becomes quite unwieldy at 100-mm working distances. Moreover, the lack of any provision for axial resolution, i.e., selection of a thin section whose diameter is to be measured, limits the usefulness of the previous diameter measurement approach for single-crystal fiber growth. The remainder of this paper describes the design of the electronic and optical systems developed to implement fiber diameter variation measurements. Experimental verification of the system performance is also presented.

II. Measurement Approach

It is possible to simplify substantially the optical system by accurately tracking the position of the center of a single fringe scattered at a large angle rather than attempting to count a large number of fringes. An anamorphic optical system can be used to obtain improved axial resolution by focusing the laser beam perpendicular to the fiber axis.

A simplified diagram of the fiber diameter measurement approach is shown in Fig. 1. A plane wave of wavelength λ illuminates the fiber. A fringe scattered at an angle θ is imaged onto a photodiode array by a lens of focal length f in a Fourier transform configuration. The center-to-center spacing of the elements of the diode array is s.

The authors are with Stanford University, Applied Physics Department, Ginzton Laboratory, Stanford, California 94305.
Received 12 March 1985.
0003-6935/85/152362-07$02.00/0.

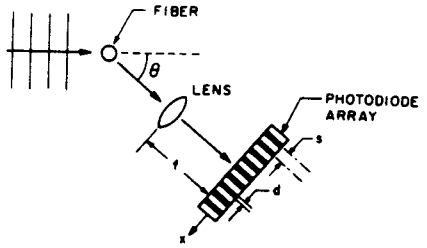

Fig. 1. Schematic of the fiber diameter measurement approach. An incident plane wave of wavelength λ scatters off a fiber. The resulting interference pattern is projected by a lens of focal length f onto a photodiode array with element spacing s and element width d.

To determine the resolution of the system, it is necessary to calculate the shift in angle of a peak due to a given change in fiber diameter.

A. Transparent Fiber

As discussed in Ref. 6, the fringe spacing of an unclad transparent fiber can be described analytically by considering the path length difference $\Lambda(\theta)$ between rays refracted through and reflected off the fiber at a given angle θ as shown in Fig. 2. The interference between these rays in the far field gives rise to a series of approximately sinusoidal fringes. The power scattered per unit angle at an angle θ can be written as

$$P(\theta) = a_1(\theta) + a_2(\theta)\cos k\Lambda(\theta), \tag{1}$$

where $k = 2\pi/\lambda$. An approximate ray optics calculation of the amplitude functions $a_1(\theta)$ and $a_2(\theta)$ is presented in the Appendix. The path length difference $\Lambda(\theta)$ is given by[6]

$$\Lambda(\theta) = 2\rho[\sin\tfrac{1}{2}\theta + (n^2 + 1 - 2n\cos\tfrac{1}{2}\theta)^{1/2}] + \lambda/4, \tag{2}$$

where n is the index of refraction of the fiber, and ρ is the fiber radius.

From Eqs. (1), (2), and (A13)–(A16) it can be shown that $a_1(\theta)$ and $a_2(\theta)$ vary sufficiently slowly that it is adequate to take the maxima of the scattering pattern to lie at the maxima of the cosine function in Eq. (1). The angular position θ_j of the jth bright fringe is then given implicitly by

$$k\Lambda(\theta_j) = 2\pi(j + j_0), \tag{3}$$

where $\Lambda(\theta = 0) = (j_0 + \delta)\lambda$, and where j_0 is an integer and $\delta < 1$.

The change in position on the diode array of the jth fringe Δx in response to a change $\Delta\rho$ in the fiber radius is

$$\Delta x = \frac{\partial\theta_j}{\partial\rho} f\Delta\rho. \tag{4}$$

With our detection system, the minimum resolvable position change is the diode spacing s. Thus the minimum resolvable radius change is

$$\Delta\rho_{\min} = \left(\frac{s}{f}\right)\left|\left(\frac{\partial\theta_j}{\partial\rho}\right)\right|^{-1}. \tag{5}$$

We can calculate $\partial\theta_j/\partial\rho$ from Eqs. (2) and (3) and find

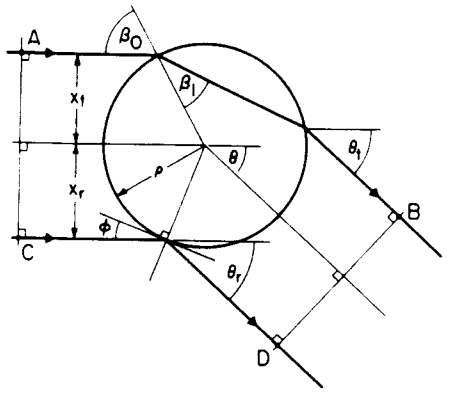

Fig. 2. Geometry of reflected and transmitted rays that interfere to form the fringe pattern. The path difference between AB and CD is given by $\Lambda(\theta)$ in Eq. (2) when $\theta_t = \theta_r = \theta$. Angles and lengths indicated are used in the Appendix to calculate scattering amplitudes $a_1(\theta)$ and $a_2(\theta)$ referred to in Eq. (1).

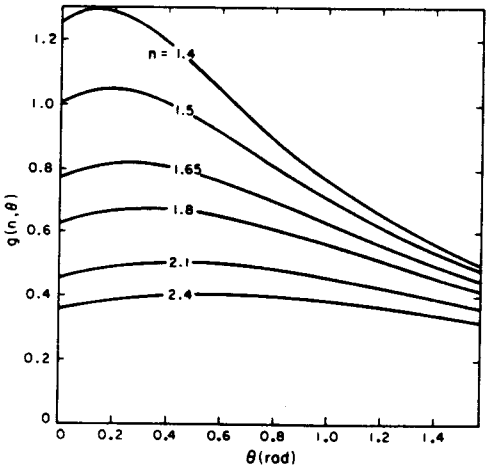

Fig. 3. Plot of sensitivity function $g(n,\theta)$ defined by Eqs. (6) and (7). Solid lines show $g(n,\theta)$ vs θ for various values of n.

$$\frac{\partial\theta_j}{\partial\rho} = \frac{-2}{\rho}\,\frac{\sin\tfrac{1}{2}\theta_j + (n^2 + 1 - 2n\cos\tfrac{1}{2}\theta_j)^{1/2}}{\cos\tfrac{1}{2}\theta_j + n(n^2 + 1 - 2n\cos\tfrac{1}{2}\theta_j)^{1/2}\sin\tfrac{1}{2}\theta_j}. \tag{6}$$

If we write this relationship in the form

$$\frac{\partial\theta_j}{\partial\rho} = -\frac{1}{\rho}g^{-1}(n,\theta_j), \tag{7}$$

we arrive at a simple form for the diameter resolution:

$$\left(\frac{\Delta\rho}{\rho}\right)_{\min} = \frac{s}{f}\,g(n,\theta_j). \tag{8}$$

The function $g(n,\theta)$ is plotted in Fig. 3 and is seen to be bounded for cases of interest by $0.3 \le g \le 1.3$.

Note also that the resolution is independent of the laser wavelength. The qualitative explanation is that for a given $\Delta\rho$, the decrease with wavelength in the number of fringes below θ_j is exactly canceled by a larger fractional shift per fringe, leading to exactly the same shift in the position of the jth peak.

For a transparent fiber with $n = 1.5$ and a measurement system with $s = 50\ \mu$m, $f = 100$ mm, and $\theta_j = 1.2$ rad, we find from Fig. 3 that $g = 0.63$ and calculate from Eq. (8) that $(\Delta\rho/\rho)_{\min} = 3.2 \times 10^{-4}$.

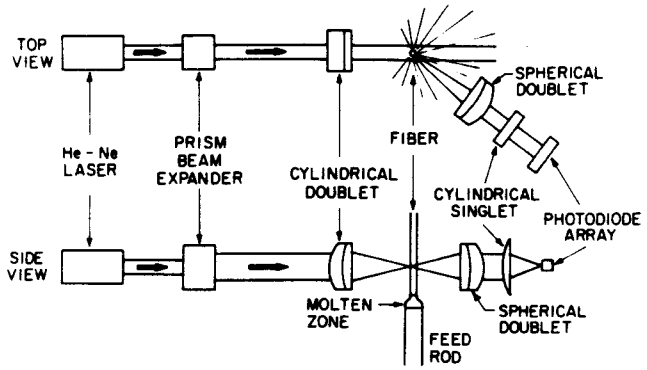

Fig. 4. Schematic diagram of the fiber diameter measurement optical system.

The dynamic range limitation occurs when the fringe moves off the diode array which consists of M elements. This occurs for $(\Delta\rho/\rho)_{max} = \pm(M/2)(s/f)g(n,\theta_j)$, where we have chosen to track the fringe originally at the center of the array.

For $M = 512$ and the other values as above, we calculate that $(\Delta\rho/\rho)_{max} = \pm 8\%$.

B. Opaque Fiber

The scattering pattern of an opaque fiber can also be written in the form of Eq. (1). It can be shown from scalar diffraction theory that for $\theta \geq \lambda/\pi w_0$, where w_0 is the beam waist in the plane perpendicular to the fiber axis, that

$$a_1(\theta) = a_2(\theta) = \frac{P_0\lambda}{2\pi^{5/2} w_0\theta^2}, \tag{9}$$

where P_0 is the incident laser power and that

$$\Lambda(\theta) = 2\rho\theta - (\lambda/2). \tag{10}$$

Since there is no refracted ray, the physical interpretation of Λ given earlier obviously no longer applies.

From Eqs. (3), (7), and (10) it is found that for an opaque fiber,

$$g(n,\theta) = g(\theta) \approx 1/\theta. \tag{11}$$

III. Optical System

A. Illumination

A block diagram of the optical system is shown in Fig. 4. The arrangement for illuminating the fiber consists of a prism beam expander and a cylindrical lens to provide the transverse focusing necessary for axial resolution. A 120-mm focal length cylindrical doublet and an input beam waist of 8 mm were chosen to meet the working distance specification and provide a line focus halfwidth of 3 μm with a He–Ne laser beam. The fiber position is tightly controlled in our apparatus, so it is not necessary to expand the beam in the direction perpendicular to the fiber axis.

B. Imaging the Fringe Pattern

The Fourier transform lens projects the fringe onto the photodiode array and determines the diameter variation resolution of the system through Eq. (8). It also serves to reduce the sensitivity of the fringe position on the diode array to movement of the fiber. In the absence of lens aberration there is no first-order variation of sensitivity across the diode array beyond that caused by $\partial g/\partial\theta$ and no first-order dependence of fringe position on the diode array on fiber position. Using a 100-mm focal length plano-convex Fourier transform lens leads to a 1% variation of sensitivity across the detector and a theoretical window for fiber motion of several hundred microns without an error of magnitude s in fringe position. A spherical doublet corrected for infinite conjugate ratio was chosen, which significantly reduces these effects as is discussed in Sec. VI.

The final cylindrical lens, in conjunction with the Fourier transform lens, concentrates the light onto the photodiode array.

IV. Electronics

The purpose of the electronic system is to lock onto one of the peaks of the interference pattern and track the location on the diode array of the center of that peak as it moves in response to diameter changes in the fiber. This task is complicated by the variations observed in peak amplitude and contrast ratio.

Figure 5 is a schematic of the electronic system designed to track an interference fringe. The output of the photodiode array, a section of which is shown in Fig. 6(a), is a series of 512 voltage levels clocked serially at a 0.5-MHz rate. The measurement is initiated by choosing a single fringe near the center of the photodiode array. The window signal [Fig. 6(b)] brackets the chosen fringe of the interference pattern and gates the boxcar integrator, whose output [Fig. 6(c)] is the average voltage of the bracketed fringe. The comparator output thus changes state on the steeply changing portions of the fringe signal. Control circuit 1 in Fig. 5 latches the output of the counter at the rising and falling edges of the comparator output that occur during the window interval. The sum of the two latch outputs thus rep-

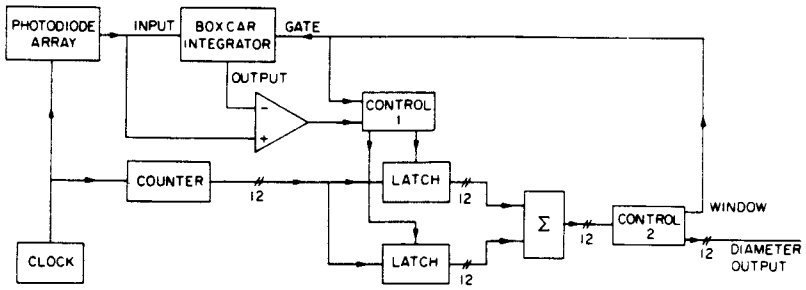

Fig. 5. Schematic diagram of the fiber diameter measurement electronic system.

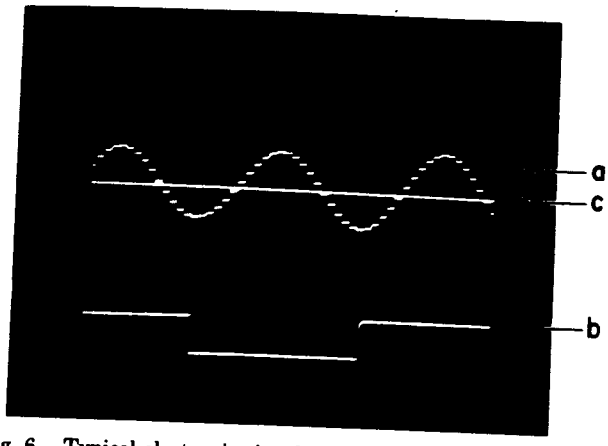

Fig. 6. Typical electronic signals: (a) output of a section of the photodiode array; (b) window signal bracketing fringe to be tracked; (c) output of boxcar integrator equal to the average value of the fringe selected by the window signal.

resents twice the value of the center of the fringe. Control circuit 2 compares this value of the center to the previous measurement. If the difference is too large, the measurement is assumed to be due to an anomalous optical or electronic event, and the output is not updated. If the new point is valid, the current fringe position measurement is transferred to the output and the window position is changed by the same increment. This cycle repeats every scan of the diode array, i.e., approximately once per millisecond.

The signal thus derived contains information only on diameter changes, not absolute diameter. If absolute diameter information were desired, additional signal processing would be necessary. At the beginning of a measurement, one absolute determination of the diameter would be made. Changes in the diameter would be measured using the technique described here. The accuracy of the diameter measurement would be determined by the accuracy of the absolute measurement technique, while the speed and resolution of the measurement would be determined by the fringe tracking system. Thus, a relatively slow method, e.g., the Fourier transform technique of Ref. 8, could be used for the absolute diameter measurement without adverse effect on the measurement rate.

V. Optimum Resolution

The linear increase in diameter resolution with the focal length of the Fourier transform lens predicted by Eq. (5) reaches an ultimate limit due to noise and nonuniform sensitivity of the elements of the photodiode array. To see where this limit occurs, it is necessary to calculate the focal length for which the difference in the output voltages of the adjacent photodiodes at the comparator threshold is less than the noise. The voltage output of the mth element of the photodiode array is given by

$$V_m = \frac{d}{f} R_m \tau P(\theta_m) + v_m, \tag{12}$$

where θ_m is the angular position of the mth element, R_m is the responsivity of the mth element (in volts per joule), τ is the measurement time interval, d is the width of an element of the array, v_m is the noise voltage on the mth element, and $P(\theta)$ is given by Eq. (1).

The difference in the output of adjacent diode elements is

$$\delta V_m = V_{m+1} - V_m \tag{13}$$

or

$$\delta V_m = \left(\frac{d}{f}\right) \tau [P(\theta_{m+1}) R_{m+1} - P(\theta_m) R_m] + (v_{m+1} - v_m). \tag{14}$$

Keeping only terms up to first order in a Taylor series expansion of $P(\theta)$ we have

$$\delta V_m = \left(\frac{d}{f}\right) \tau \left[\frac{s}{f} R_m \left.\frac{dP}{d\theta}\right|_{\theta_m} + (R_{m+1} - R_m) P(\theta_m)\right] + (v_{m+1} - v_m). \tag{15}$$

The first term in Eq. (15) can be evaluated from Eq. (1). If we assume $da_1/d\theta \ll a_2 k \partial\Lambda/\partial\theta$, we have

$$\delta V = U + E, \tag{16}$$

where

$$U = \frac{sd}{f^2} \tau R_m a_2(\theta_m) k \left.\frac{d\Lambda}{d\theta}\right|_{\theta_m},$$

$$E = \frac{d}{f} \tau (R_{m+1} - R_m) a_1(\theta_m) + (v_{m+1} - v_m).$$

The first term U in Eq. (16) is the result for an ideal noiseless uniform diode array, while E represents deviations due to nonuniform response and noise. Note that U decreases more rapidly with f than does E. If f_{opt} is chosen so that $U = E$, there is a one-diode uncertainty in the location of the peak center. Thus we can find the optimum focal length f_{opt} for a given observation angle θ by solving

$$U(f_{\text{opt}}, \theta) = E(f_{\text{opt}}, \theta). \tag{17}$$

Noting the relation between $(\Delta\rho/\rho)$ and f_{opt} given in Eq. (8) and using Eqs. (16), (17), and (A12), we obtain a quadratic equation for the maximum usable resolution at a given angle:

$$0 = -[\bar{a}_2 h(\theta)/g^2](\Delta\rho/\rho)^2 + (\bar{a}_1/2\pi g)(\delta R/R)(\lambda/\rho)(\Delta\rho/\rho) + (2\sqrt{2\pi})^{-1}(E_0/P_0\tau)(s/d)(w_0/\rho)(\lambda/\rho), \tag{18}$$

where $\delta R/R$ is the fractional variation of the photodiode responsivity and

$$h(\theta) = \frac{1}{\rho} \frac{\partial\Lambda}{\partial\theta}$$

$$= \cos(\tfrac{1}{2}\theta) + n \sin(\tfrac{1}{2}\theta)(n^2 + 1 - 2n \cos\tfrac{1}{2}\theta)^{-1/2}.$$

Here $E_0 = R_m v_m$ is a noise equivalent energy, and $\bar{a}_1$ and $\bar{a}_2$ are the dimensionless scattering coefficients defined in Eqs. (A13) and (A14). Solving Eq. (18) for $(\Delta\rho/\rho)$ and minimizing the result with respect to θ yield θ_{opt}, the optimum θ for a given experimental situation. Substituting θ_{opt} into Eq. (18) yields $(\Delta\rho/\rho)_{\text{opt}}$, the optimum resolution.

Figure 7 plots θ_{opt} vs the log of a dimensionless parameter ϵ defined by

$$\epsilon = (2\pi^3)^{-1/4} \left(\frac{\delta R}{R}\right) \left(\frac{P_0\tau}{E_0} \frac{d}{s} \frac{\lambda}{w_0}\right)^{1/2}, \tag{19}$$

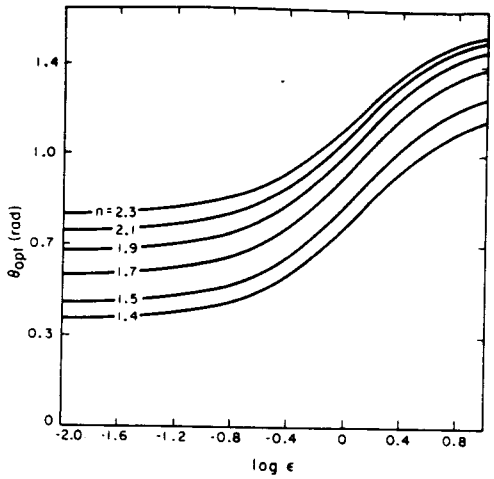

Fig. 7. Scattering angle for highest resolution for several values of n vs logϵ, where ϵ is a dimensionless parameter defined by Eq. (19) characterizing the relative importance of nonuniform photodiode responsivity and noise. Note that the optimum angle is not a function of fiber diameter.

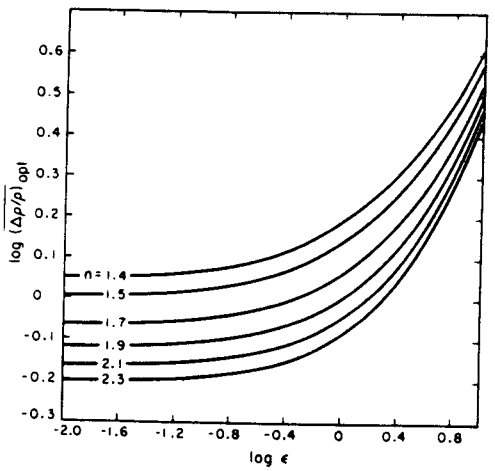

Fig. 8. Logarithm of normalized optimized resolution $\overline{(\Delta\rho/\rho)}_{opt}$ [defined by Eq. (20)] for several values of n vs logϵ. [ϵ is defined by Eq. (19).]

which characterizes the relative importance of nonuniform responsivity and noise of the photodiode array. For large ϵ, i.e., for cases where noise is unimportant, θ_{opt} approaches large values, where the fringe contrast is maximum while for small ϵ, i.e., for cases where nonuniformity is unimportant, θ_{opt} approaches smaller values where the intensity of the fringes is maximum. The normalized optimum resolution as defined by

$$\overline{(\Delta\rho/\rho)}_{opt} = (\Delta\rho/\rho)_{opt}\left(2\sqrt{2\pi}\,\frac{P_0\tau}{E_0}\,\frac{d}{s}\,\frac{\rho}{w_0}\,\frac{\rho}{\lambda}\right)^{1/2} \tag{20}$$

is plotted in Fig. 8.

For $P_0 = 2$ mW, $\tau = 1$ msec, $E_0 = 0.1$ pJ, $d/s = 1$, $w_0 = 0.8$ mm, $\rho = 0.1$ mm, $n = 1.5$, $\delta R/R = 0.05$, and other diode array parameters as in the previous example, we calculate $\theta_{opt} = 1$ rad, $(\Delta\rho/\rho)_{opt} = 4 \times 10^{-5}$, $g(1.5,\theta_{opt}) = 0.71$, and $f_{opt} = 0.89$ m.

Equation (17) can also be solved for an opaque fiber using Eqs. (9), (10), and (16). For cases of interest the diode noise effects are much more important than the nonuniformity. In this limit the optimum resolution is given by

$$\left(\frac{\Delta\rho}{\rho}\right)_{opt} = \frac{\pi}{2}\left(\frac{E_0}{P_0\tau}\,\frac{w_0}{\rho}\,\frac{s}{d}\right)^{1/2}. \tag{21}$$

Note that these resolutions are a theoretical upper bound. Various practical considerations, such as lens aberrations, minimum acceptable dynamic range, background light, and adaptability to a variety of fibers and diameters, are often more serious limits than the diode noise and nonuniformity.

VI. Experimental Results

The apparatus was set up as described in the previous sections. The photodiode array consisted of 512 elements that were 25 μm wide and on 50-μm centers. The array was clocked at a 0.5-MHz rate so that one scan was completed in 1 msec. The focal length of both the cylindrical and Fourier transforming lenses was 120 mm. This latter value was a compromise between a number of conflicting criteria and, therefore, did not coincide with the focal length that would provide the optimum resolution. A variable attenuator was inserted between the 2-mW He–Ne laser and the beam expander to prevent saturation of the photodiode array. Typically the laser power was in the 0.5–1.5-mW range. Measurements were made at θ values of 24 and 63°.

The scale factor g given by Eq. (8) was checked by using an optical microscope. We measured the diameter vs position along several tapered fibers using both the fringe tracking system and an optical microscope. An experimental g factor was obtained by fitting the fringe tracker results to the microscope measurements. For both sapphire ($n = 1.76$) and glass ($n = 1.47$) fibers, at both $\theta = 24°$ and $\theta = 63°$, and for diameters ranging from 100 to 350 μm, the experimental g factor agreed with the theoretical result, Eqs. (6) and (7), to better than 10%. For example, the measured g factor at $\theta = 63°$ was 0.68 ± 0.07 for a glass fiber with $n = 1.47$, while the g factor calculated with Eq. (8) was 0.71. Small discrepancies may have occurred due to the slight ellipticity of the glass fibers or the slightly hexagonal shape of the sapphire fibers.

The output of the diameter measurement system was monotonic plus or minus a one-bit jitter for scans of a smoothly tapered glass fiber. Since the output of the fringe tracker was monotonic, and the experimental and theoretical g factors were in good agreement, it is reasonable to assume that the resolution is given correctly by Eq. (8) for our experimental arrangement.

Figure 9 shows a scan of a 350-μm diam glass fiber compared to measurements made using an optical microscope. Figure 10 shows a scan of a 50-μm diam ruby fiber grown by the crystal growth apparatus under open-loop conditions.

A constant diameter glass fiber was mounted on an x-y stage to measure errors due to motion in the plane perpendicular to the fiber axis. At both the 24 and 63° measurement angles a one-bit error window of 11 mm along the axis of the incident beam and 1.5 mm perpendicular to the axis of the incident beam was mea-

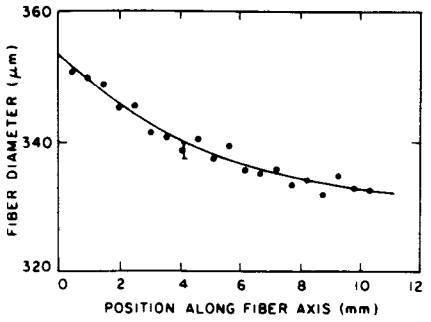

Fig. 9. Diameter vs length of a 350-μm diam glass fiber. The solid line was measured using the fringe tracking apparatus; the closed circles were measured using an optical microscope.

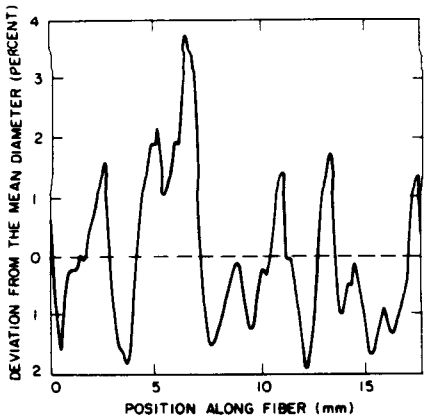

Fig. 10. Diameter change vs length for a 50-μm diam ruby fiber grown under open-loop conditions by the fiber growth apparatus described in Ref. 1.

sured. The former limit is due to lens aberration, while the latter is due to curvature of the phase front of the He–Ne beam in the direction perpendicular to the fiber axis. This latter window could be enlarged by collimation of the beam in that direction.

VII. Conclusion

We have designed and built a fiber diameter variation measurement system which has measured the diameter variation of transparent fibers having diameters between 25 and 300 μm, with 0.02% diam resolution and 6-μm axial resolution at a 1-kHz measurement rate and with a working distance of >100 mm. Modifications, such as a longer focal length Fourier transform lens, could increase the diameter resolution by 1 order of magnitude. This device is being used to provide real time measurements of the diameter variation of single-crystal refractory oxide fibers during growth.

The authors are grateful to Michel Digonnet and Keith Bennett for many helpful suggestions. Gregory Magel gratefully acknowledges the support of the Fannie and John Hertz Foundation. This work was supported by the U.S. Air Force under contract F49620-84-C-0021 and by the Joint Services Electronics Program under contract N00014-84-K-0327.

Appendix: Ray Calculation of Fringe Amplitudes

To obtain the amplitude of the fringe pattern of a transparent fiber, it is necessary to combine the amplitudes of the reflected and refracted rays, taking into account the phase difference between them.[9] The power scattered between θ and $\theta + d\theta$ is given by

$$P(\theta) = P_r(\theta) + P_t(\theta) + 2\sqrt{P_r(\theta)P_t(\theta)}\cos k\Lambda(\theta), \quad \text{(A1)}$$

where $P_r(\theta)$ and $P_t(\theta)$ are the power per unit angle in the reflected and transmitted rays, respectively.

We assume the geometry shown in Fig. 2 with a uniform incident power per unit length I to obtain P_r and P_t. From conservation of energy it is clear that

$$P_r(\theta) = I\mathcal{R}(\theta)\left|\frac{dx_r(\theta)}{d\theta_r}\right|, \quad \text{(A2)}$$

$$P_t(\theta) = I\mathcal{T}(\theta)\left|\frac{dx_t(\theta)}{d\theta_t}\right|, \quad \text{(A3)}$$

where $\mathcal{R}(\theta)$ and $\mathcal{T}(\theta)$ are the power reflection and transmission coefficients.

If we assume that the incident beam of total power P_0 is Gaussian with a halfwidth w_0, which is much larger than the fiber radius a, then $I = (2/\pi)^{1/2}(P_0/w_0)$. The necessary geometrical relationships to calculate the other quantities appearing in Eqs. (A2) and (A3) can be obtained from Fig. 2 and Snell's law. We see that

$$\frac{d\phi}{dx_r} = \frac{-1}{\rho\sin\phi}. \quad \text{(A4)}$$

Since $\theta_r = 2\phi$, we can immediately write

$$\left.\frac{d\theta_r}{dx_r}\right|_{\theta_r=\theta} = \frac{-2}{\rho\sin\frac{1}{2}\theta_r}. \quad \text{(A5)}$$

Noticing that

$$\theta_t = 2(\beta_0 - \beta_1), \quad \text{(A6)}$$

where

$$\beta_1 = \sin^{-1}(x_t/n\rho), \quad \text{(A7)}$$

$$\beta_0 = \sin^{-1}(x_t/\rho), \quad \text{(A8)}$$

we obtain

$$\left.\frac{d\theta_t}{dx_t}\right|_{\theta_t=\theta} = \frac{2}{\rho}\left(\frac{1}{\cos\beta_0} - \frac{1}{n\cos\beta_1}\right). \quad \text{(A9)}$$

$\mathcal{R}$ and $\mathcal{T}$ can now be obtained from Fresnel's equations. Assuming the incident light to be polarized parallel to the fiber axis, we have

$$\mathcal{R}(\theta) = \left(\frac{\sin\frac{1}{2}\theta - n\cos\gamma}{\sin\frac{1}{2}\theta + n\cos\gamma}\right)^2, \quad \text{(A10)}$$

$$\mathcal{T}(\theta) = \left[\frac{4n\cos\beta_0\cos\beta_1}{(\cos\beta_0 + n\cos\beta_1)^2}\right]^2, \quad \text{(A11)}$$

where $\gamma \equiv \sin^{-1}[(1/n)\cos\frac{1}{2}\theta]$.

Finally, we can combine Eqs. (A1)–(A11) to obtain

$$P(\theta) = P_0\left(\frac{2}{\pi}\right)^{1/2}\left(\frac{\rho}{w_0}\right)[\bar{a}_1(\theta) + \bar{a}_2(\theta)\cos k\Lambda(\theta)], \quad \text{(A12)}$$

where $\bar{a}_1(\theta)$ and $\bar{a}_2(\theta)$ are given by the following equations:

$$\bar{a}_1(\theta) = \tfrac{1}{2}\left[\mathcal{R}(\theta)\sin(\tfrac{1}{2}\theta) + \mathcal{T}(\theta)\left(\frac{1}{\cos\beta_0} - \frac{1}{n\cos\beta_1}\right)^{-1}\right]; \quad \text{(A13)}$$

$$\bar{a}_2(\theta) = \left[\mathcal{R}(\theta)\mathcal{T}(\theta)\ \sin(\tfrac{1}{2}\theta)\left(\frac{1}{\cos\beta_0} - \frac{1}{n\cos\beta_1}\right)^{-1}\right]^{1/2}. \quad \text{(A14)}$$

The fringe amplitude coefficients a_1 and a_2 appearing in Eq. (1) in Sec. II are then given by

$$a_1(\theta) = P_0\left(\frac{2}{\pi}\right)^{1/2}\left(\frac{\rho}{w_0}\right)\bar{a}_1(\theta), \quad \text{(A15)}$$

$$a_2(\theta) = P_0\left(\frac{2}{\pi}\right)^{1/2}\left(\frac{\rho}{w_0}\right)\bar{a}_2(\theta). \quad \text{(A16)}$$

These results are also used in Sec. V to calculate the optimum resolution of the diameter measurement system.

References

1. M. M. Fejer, J. L. Nightingale, G. A. Magel, and R. L. Byer, "Laser Heated Miniature Pedestal Growth Apparatus for Single Crystal Optical Fibers," Rev. Sci. Instrum. **55**, 1791 (1984).
2. J. Stone and C. A. Burrus, "Self Contained LED-Pumped Single Crystal Nd:YAG Fiber Lasers," Fiber Integrated Opt. **2**, 19 (1979).
3. T. J. Bridges, J. S. Hasiak, and A. R. Strand, "Single Crystal AgBr Infrared Optical Fibers," Opt. Lett. **5**, 85 (1980).
4. G. D. Boyd, L. A. Coldren, and R. N. Thurston, "Acoustic Clad Fiber Delay Lines," IEEE Trans. Sonics Ultrason. **SU-24**, 246 (1977).
5. C. A. Burrus and J. Stone, "Single Crystal Fiber Optical Devices: A Nd:YAG Fiber Laser," Appl. Phys. Lett. **26**, 318 (1975).
6. L. S. Watkins, "Scattering from Side-Illuminated Clad Class Fibers for Determination of Fiber Parameters," J. Opt. Soc. Am. **64**, 767 (1974).
7. D. H. Smithgall, L. S. Watkins, and R. E. Frazee, Jr., "High-Speed Noncontact Fiber-Diameter Measurement Using Forward Light Scattering," Appl. Opt. **16**, 2395 (1977).
8. M. A. G. Abushagur and N. George, "Measurement of Optical Fiber Diameter Using the Fast Fourier Transform," Appl. Opt. **19**, 2031 (1980).
9. A similar analysis for determination of fiber location in silicone coatings appears in D. H. Smithgall, "Light Scattering Model for the Determination of Fiber Location in Silicone Coatings," Appl. Opt. **21**, 1326 (1982).